Transient Primary Control Effort of AC Electric Power Networks under Line Contingencies

T. Coletta and Ph. Jacquod *

* *School of Engineering, University of Applied Sciences of Western Switzerland, CH-1951 Sion, Switzerland (e-mail: {tommaso.coletta,philippe.jacquod}@hevs.ch).*

Abstract: Classes of performance measures have been recently introduced to quantify the response of network-coupled dynamical systems to external disturbances. So far, investigations of these performance measures have been restricted to nodal disturbances. Here, we go beyond earlier works and consider the equally important, but so far neglected case of a line fault. We find that, within the DC power flow approximation, the transient primary control effort necessary to restore synchrony depends on whether the faulted line connects two passive, two active buses or one active to one passive bus. In all cases, performance measures depend quadratically on the original load on the faulted line multiplied by an inertia-dependent prefactor. When the faulted line is connected to at least one passive bus, this inertia-dependent prefactor further depends on the topology of the network. The procedure allows to rank lines in increasing order of the network response to their removal. Quite unexpectedly, we find that the most critical lines, corresponding to the largest network response, are not always those carrying the largest power flows, and that faulting moderately loaded lines often leads to large response due to the topology dependent prefactor. Our theoretical formalism is restricted to Dirac-δ perturbations and we investigate numerically the validity of our results for finite-time line faults. We find good agreement with theoretical predictions for longer fault durations in systems with more inertia.

Keywords: Power generation control, power system dynamics performance measures, line contingency.

1. INTRODUCTION

In normal operation, electric power grids are synchronized. Their operating state corresponds to equal frequencies and voltage angle differences ensuring power conservation at all buses. Such synchronous states are not specific to power grids. They occur in many different coupled dynamical systems, depending on the balance between the internal dynamics of the individual systems and the coupling between them (Kuramoto, 1975; Pikovsky et al., 2001). For the specific case of electric power grids, the individual systems are either generators or loads, and they are coupled to one another by power lines. Individual units have effective internal dynamics determined by their nature – they may be rotating machines, inertialess new renewable energy sources, load impedances and so forth – and by the amount of power they generate or consume (Machowski et al., 2008). Rapid changes are currently affecting electric power grids and impact their operating state. It is in particular expected that future power grids will be subjected more often to stronger external perturbations to which they may react more strongly (Backhaus and Chertkov, 2013; Rohden et al., 2014). There is therefore a clear need to better assess power grid vulnerability and quantify their response to external disturbances.

⋆ This work has been supported by the Swiss National Science Foundation under an AP energy grant.

Investigations have been initiated on the robustness of the synchronous operating state of electric power grids against perturbations such as fluctuating feed-in or sudden power losses. An appealing approach has been proposed (Bamieh et al., 2012; Summers et al., 2015; Siami and Motee, 2016; Fardad et al., 2014; Tyloo et al., 2018), which starts from a stable operating state, perturbs it and quantifies the magnitude of the induced transient excursion through various performance measures. Focusing on Dirac-δ, nodal perturbations – instantaneous changes in generation or consumption – quadratic performance measures have been proposed, which can be formulated as $\mathcal{L}_2$ and squared $\mathcal{H}_2$ norms of linear systems. The approach is mathematically elegant because these norms can be conveniently expressed in terms of observability Gramians (Zhou et al., 1996). These performance measures allow to evaluate additional transient transmission losses incurred during the transient as synchronous machines oscillate relative to one another (Bamieh and Gayme, 2013; Tegling et al., 2015; Grunberg and Gayme, 2016), the primary control effort necessary to restore synchrony (Poolla et al., 2017) or the coherence of the system (Bamieh et al., 2012). Under the assumptions that synchronous machines have uniform inertia and damping coefficients, and that transmission lines are homogeneous – that they have constant resistance over reactance ratios – Bamieh and Gayme (2013) obtained that additional transmission losses depend only on the

number of buses in the network, and not on its topology. This result is rather puzzling – can it be that a network's performance depends only on the number of its nodes and not on the way they are connected ? Further investigations however showed that transient transmission losses strongly depend on the homogeneous line assumption, and that when the latter is relaxed, they do depend on topological details (Tegling et al., 2015; Grunberg and Gayme, 2016) and are in particular related to a graph theoretical distance metric known as the resistance distance (Klein and Randić, 1993; Stephenson and Zelen, 1989).

To the best of our knowledge, investigations of performance measures of synchronized states have considered nodal perturbations only. Our contribution in this paper is to extend these earlier investigations to line contingencies which are at least as important for evaluating the robustness of electric power grids as nodal disturbances. We find that the network topology is quite important in determining which line fault results in the strongest response. In particular, faults on moderately loaded lines may lead to the strongest responses.

2. MATHEMATICAL NOTATION

Given a vector $\boldsymbol{v} \in \mathbb{R}^N$ and a matrix $\boldsymbol{M} \in \mathbb{R}^{N\times N}$ we denote their transpose by $\boldsymbol{v}^\top$ and $\boldsymbol{M}^\top$. For any two vectors $\boldsymbol{u}, \boldsymbol{v} \in \mathbb{R}^N$, $\boldsymbol{u}\boldsymbol{v}^\top \in \mathbb{R}^{N\times N}$ is a matrix with components $u_i v_j$, furthermore we write $\mathrm{diag}(\{v_i\})$ for the diagonal matrix with diagonal entries $v_1, \dots, v_N$. Let $\boldsymbol{e}_l \in \mathbb{R}^N$ with $l \in \{1, \dots, N\}$ be the unit vector with components $(e_l)_i = \delta_{il}$, we define $\boldsymbol{e}_{(l,q)} \in \mathbb{R}^N$ as $\boldsymbol{e}_{(l,q)} = \boldsymbol{e}_l - \boldsymbol{e}_q$.

We consider undirected weighted graphs $\mathcal{G}$ with N vertices, and a set of edge weights $\{w_{ij}\}$ with $w_{ij} = 0$ whenever i and j are not connected by an edge, and $w_{ij} = w_{ji} > 0$ otherwise. The graph Laplacian $\boldsymbol{L} \in \mathbb{R}^{N\times N}$ is the symmetric matrix $\boldsymbol{L} = \sum_{i<j} w_{ij} \boldsymbol{e}_{(i,j)} \boldsymbol{e}_{(i,j)}^\top$, with eigenvalues $\{\lambda_1, \dots \lambda_N\}$ and orthonormal eigenvectors $\{\boldsymbol{u}^{(1)}, \dots, \boldsymbol{u}^{(N)}\}$. The zero row and column sum property of $\boldsymbol{L}$ implies that $\lambda_1 = 0$ and that ${\boldsymbol{u}^{(1)}}^\top = (1, \dots, 1)/\sqrt{N}$. In connected graphs, $\lambda_i > 0$ for $i = 2, \dots, N$. The Moore-Penrose pseudoinverse $\boldsymbol{L}^\dagger$ of $\boldsymbol{L}$ has eigenvalues $\{0, \lambda_2^{-1}, \dots, \lambda_N^{-1}\}$ and is such that $\boldsymbol{L}\boldsymbol{L}^\dagger = \boldsymbol{L}^\dagger\boldsymbol{L} = \mathbb{I} - \boldsymbol{u}^{(1)}{\boldsymbol{u}^{(1)}}^\top$ with the identiy matrix $\mathbb{I} \in \mathbb{R}^{N\times N}$.

The effective resistance distance between any two nodes i and j of the network is defined as $\Omega_{ij} = \boldsymbol{e}_{(i,j)}^\top \boldsymbol{L}^\dagger \boldsymbol{e}_{(i,j)}$ (Klein and Randić, 1993; Stephenson and Zelen, 1989). This quantity is a graph theoretical distance metric satisfying the properties: i) $\Omega_{ii} = 0\ \forall i$, ii) $\Omega_{ij} \geq 0\ \forall i \neq j$, and iii) $\Omega_{ij} \leq \Omega_{ik} + \Omega_{kj}\ \forall i, j, k$. It is known as the *resistance* distance because if one replaces the edges of $\mathcal{G}$ by resistors with a conductance $1/R_{ij} = w_{ij}$, then Ω_{ij} is equal to the equivalent network resistance when a current is injected at node i and extracted at node j with no injection anywhere else. The resistance distance can be written $\Omega_{ij} = \sum_{l\geq 2} \lambda_l^{-1} (u_i^{(l)} - u_j^{(l)})^2$, in terms of the eigenvalues and eigenvectors of $\boldsymbol{L}$ (Klein, 1997; Xiao and Gutman, 2003; Coletta and Jacquod, 2017).

3. POWER NETWORK MODEL AND QUADRATIC PERFORMANCE MEASURES

We consider the dynamics of high voltage transmission power networks in the DC power flow approximation. This approximation of the full nonlinear dynamics assumes uniform and constant voltage magnitudes, purely susceptive transmission lines and small voltage phase differences. The steady state power flow equations relating the active power injections $\boldsymbol{P}$ to the voltage phases $\boldsymbol{\theta}$ at every node read $\boldsymbol{P} = \boldsymbol{L_b}\boldsymbol{\theta}$, with the Laplacian $\boldsymbol{L_b}$ of the graph modeling the electric network, with edge weights given by the susceptances of the transmission lines $w_{ij} = b_{ij} \geq 0$. We assume that each node of the network has a synchronous machine (generator or consumer) of rotational inertia $m_i > 0$ and damping coefficient $d_i > 0$. A further assumption we make is that all synchronous machines have uniform damping over inertia ratios $d_i/m_i = \gamma > 0,\ \forall i$. This assumption is a standard one when analytically calculating performance measures (2) (Bamieh et al., 2012; Bamieh and Gayme, 2013; Tegling et al., 2015; Grunberg and Gayme, 2016; Poolla et al., 2017; Paganini and Mallada, 2017). Machine measurements indicate that the ratio d_i/m_i varies by about an order of magnitude from rotating machine to rotating machine (Kou et al., 2013), so that this assumption, while strictly speaking not justified, is not unrealistic.

For constant voltages, the network dynamics is governed by the *swing* equations (Machowski et al., 2008). In the frame rotating at the nominal frequency of the network, and in the DC approximation, they read

$$\boldsymbol{M}\ddot{\boldsymbol{\theta}} = -\boldsymbol{D}\dot{\boldsymbol{\theta}} + \boldsymbol{P} - \boldsymbol{L_b}\boldsymbol{\theta}, \tag{1}$$

with $\boldsymbol{M} = \mathrm{diag}(\{m_i\})$ and $\boldsymbol{D} = \mathrm{diag}(\{d_i\})$. Subject to a disturbance such as a power injection perturbation or a line fault, the system deviates from the equilibrium operating point $(\boldsymbol{\theta}^\star, \boldsymbol{\omega}) := (\boldsymbol{L_b}^\dagger \boldsymbol{P}, 0)$ according to $\boldsymbol{\theta}(t) = \boldsymbol{\theta}^\star + \boldsymbol{\varphi}(t)$, and $\boldsymbol{\omega}(t) = \dot{\boldsymbol{\varphi}}(t)$. For asymptotically stable systems and perturbations that are short and weak enough that they leave the dynamics inside the basin of attraction of $\boldsymbol{\theta}^\star$, the operating point will eventually return to $(\boldsymbol{\varphi}, \boldsymbol{\omega}) = (0, 0)$. We quantify the transient excursion via quadratic performance measures of the kind

$$\mathcal{P} = \int_0^\infty \left[\, \boldsymbol{\varphi}^\top \boldsymbol{\omega}^\top \,\right] \boldsymbol{Q} \begin{bmatrix} \boldsymbol{\varphi} \\ \boldsymbol{\omega} \end{bmatrix} \mathrm{d}t\,, \quad \boldsymbol{Q} = \begin{bmatrix} \boldsymbol{Q}^{(1,1)} & 0 \\ 0 & \boldsymbol{Q}^{(2,2)} \end{bmatrix}, \tag{2}$$

where the disturbance starts at $t = 0$ and the symmetric matrix $\boldsymbol{Q} \in \mathbb{R}^{2N\times 2N}$ depends on the chosen performance measure. In this manuscript, we discuss the case $\boldsymbol{Q}^{(1,1)} = 0$ and $\boldsymbol{Q}^{(2,2)} = \boldsymbol{D}$, corresponding to $\mathcal{P} = \int_0^\infty \sum_i d_i \omega_i^2 \,\mathrm{d}t$, i.e. a measure of the primary control effort necessary to resynchronize the system (Poolla et al., 2017).

4. PERFORMANCE MEASURES UNDER LINE CONTINGENCIES: FORMALISM

In power networks, some nodes have no dynamics of their own. They are called *passive* nodes. A procedure called Kron reduction allows to eliminate these nodes and to formulate the dynamics of the network in terms of swing equations, similar to (1), involving only the voltage angles of the synchronous machines, all with a finite inertia (Dörfler and Bullo, 2013). The obtained swing equations is defined on an effective, Kron reduced network,

which is usually very different from the real, physical network. We therefore distinguish between Laplacians of the physical and Kron reduced networks: the physical Laplacians are $\boldsymbol{L}_{\boldsymbol{b}}^{(0)}$ (prior to the line fault) and $\boldsymbol{L}_{\boldsymbol{b}}$ (after the line fault) and the Kron reduced Laplacian is $\boldsymbol{L}_{\rm red}$.

Let $\mathcal{N}_g = \{1, \dots, g\}$ and $\mathcal{N}_c = \{g+1, \dots, N\}$ be the node subsets representing synchronous machines and passive nodes respectively, we write the DC power flow equation in the physical network as

$$\begin{bmatrix} \boldsymbol{P}_g \\ \boldsymbol{P}_c \end{bmatrix} = \underbrace{\begin{bmatrix} \boldsymbol{L}_{\boldsymbol{b}}^{gg} & \boldsymbol{L}_{\boldsymbol{b}}^{gc} \\ \boldsymbol{L}_{\boldsymbol{b}}^{cg} & \boldsymbol{L}_{\boldsymbol{b}}^{cc} \end{bmatrix}}_{\boldsymbol{L}_{\boldsymbol{b}}^{(0)}} \begin{bmatrix} \boldsymbol{\theta}_g^\star \\ \boldsymbol{\theta}_c^\star \end{bmatrix}, \tag{3}$$

where $\boldsymbol{L}_{\boldsymbol{b}}^{gg}, \boldsymbol{L}_{\boldsymbol{b}}^{gc}, \boldsymbol{L}_{\boldsymbol{b}}^{cg}$ and $\boldsymbol{L}_{\boldsymbol{b}}^{cc}$ are blocks of the physical Laplacian $\boldsymbol{L}_{\boldsymbol{b}}^{(0)}$. Applying Kron reduction to (3) to eliminate $\boldsymbol{\theta}_c^\star$ gives

$$\underbrace{\boldsymbol{P}_g - \boldsymbol{L}_{\boldsymbol{b}}^{gc}[\boldsymbol{L}_{\boldsymbol{b}}^{cc}]^{-1}\boldsymbol{P}_c}_{\boldsymbol{P}_{\rm red}} = \underbrace{\left[\boldsymbol{L}_{\boldsymbol{b}}^{gg} - \boldsymbol{L}_{\boldsymbol{b}}^{gc}[\boldsymbol{L}_{\boldsymbol{b}}^{cc}]^{-1}\boldsymbol{L}_{\boldsymbol{b}}^{cg}\right]}_{\boldsymbol{L}_{\rm red}} \boldsymbol{\theta}_g^\star . \tag{4}$$

Starting from the physical injections $\boldsymbol{P}_g$, $\boldsymbol{P}_c$ and the physical network with Laplacian $\boldsymbol{L}_{\boldsymbol{b}}$, (4) defines an effective vector of power injections $\boldsymbol{P}_{\rm red}$ and an effective Laplacian $\boldsymbol{L}_{\rm red}$ on a reduced graph (Dörfler and Bullo, 2013). The swing dynamics on the reduced graph reads

$$\boldsymbol{M}\ddot{\boldsymbol{\theta}}_g = -\boldsymbol{D}\dot{\boldsymbol{\theta}}_g + \boldsymbol{P}_{\rm red} - \boldsymbol{L}_{\rm red}\boldsymbol{\theta}_g, \tag{5}$$

with $\boldsymbol{M} = \mathrm{diag}(\{m_i\})$ and $\boldsymbol{D} = \mathrm{diag}(\{d_i\})$ for $i \in \mathcal{N}_g$. Because Kron reduction has eliminated all passive nodes, all remaining nodes have inertia and their dynamics is governed by (5).

We next consider nonsingular single line faults that do not split the physical network into two disconnected parts. The fault is modeled by a time dependent network (physical, i.e. not Kron-reduced) Laplacian

$$\boldsymbol{L}_{\boldsymbol{b}}(t) = \boldsymbol{L}_{\boldsymbol{b}}^{(0)} - \delta(t)\,\tau\, b_{\alpha\beta}\boldsymbol{e}_{(\alpha,\beta)}\boldsymbol{e}_{(\alpha,\beta)}^\top , \tag{6}$$

where $\boldsymbol{e}_{(\alpha,\beta)} \in \mathbb{R}^{|\mathcal{N}_g|+|\mathcal{N}_c|}$ and τ is introduced for dimensionality purposes. Equation (6) describes an infinitesimally short line fault at $t = 0$. We assume that the fault does not drive the transient dynamics outside the basin of attraction of the nominal operating point, and that the linearized swing dynamics still holds under such contingency.

To characterize the transient behavior resulting from a line contingency, we first need to formulate how a line fault (6) in the physical network impacts the swing dynamics of the Kron reduced network (5). This analysis requires to distinguish three cases, which we treat sequentially.

The faulted line connects two synchronous machines. In this case $\alpha, \beta \in \mathcal{N}_g$ and the fault (6) only affects the $\boldsymbol{L}_{\boldsymbol{b}}^{gg}$ block of the Laplacian [see (3)]. In terms of $\boldsymbol{L}_{\rm red}$ and $\boldsymbol{P}_{\rm red}$ the fault is described by

$$\boldsymbol{P}_{\rm red} \to \boldsymbol{P}_{\rm red}\,, \qquad \boldsymbol{L}_{\rm red} \to \boldsymbol{L}_{\rm red} - \delta(t)\,\tau\, b_{\alpha\beta}\boldsymbol{e}_{(\alpha,\beta)}\boldsymbol{e}_{(\alpha,\beta)}^\top , \tag{7}$$

where $\boldsymbol{e}_{(\alpha,\beta)} \in \mathbb{R}^{|\mathcal{N}_g|}$. The swing equations (5), relative to the nominal operating point $\boldsymbol{\theta}_g(t) = \boldsymbol{\theta}_g^\star + \boldsymbol{\varphi}_g(t)$, become

$$\boldsymbol{M}\ddot{\boldsymbol{\varphi}}_g = -\boldsymbol{D}\dot{\boldsymbol{\varphi}}_g - \boldsymbol{L}_{\rm red}\boldsymbol{\varphi}_g + \delta(t)\,\tau\, b_{\alpha\beta}\boldsymbol{e}_{(\alpha,\beta)}\boldsymbol{e}_{(\alpha,\beta)}^\top(\boldsymbol{\theta}_g^\star + \boldsymbol{\varphi}_g)\,, \tag{8}$$

where the subscript g indicates that after the Kron reduction, only angle and frequency on active nodes are considered. With the initial condition $(\overline{\boldsymbol{\varphi}}_g(0), \overline{\boldsymbol{\omega}}_g(0)) = (0, 0)$, the solution to Eq. (8) is

$$\begin{bmatrix} \overline{\boldsymbol{\varphi}}_g(t) \\ \overline{\boldsymbol{\omega}}_g(t) \end{bmatrix} = e^{\boldsymbol{A}t} \underbrace{\begin{bmatrix} 0 \\ \boldsymbol{M}^{-1/2} b_{\alpha\beta}\,\tau\, \boldsymbol{e}_{(\alpha,\beta)}\boldsymbol{e}_{(\alpha,\beta)}^\top \boldsymbol{\theta}_g^\star \end{bmatrix}}_{\boldsymbol{B}}, \tag{9}$$

where, following (Paganini and Mallada, 2017) we used rescaled angles and frequencies, $\overline{\boldsymbol{\varphi}}_g = \boldsymbol{M}^{1/2}\boldsymbol{\varphi}_g$, $\overline{\boldsymbol{\omega}}_g = \boldsymbol{M}^{1/2}\boldsymbol{\omega}_g$, and

$$\boldsymbol{A} = \begin{bmatrix} 0 & \mathbb{I} \\ -\boldsymbol{M}^{-1/2}\boldsymbol{L}_{\rm red}\boldsymbol{M}^{-1/2} & -\boldsymbol{M}^{-1}\boldsymbol{D} \end{bmatrix}. \tag{10}$$

The faulted line connects two passive nodes. In this case $\alpha, \beta \in \mathcal{N}_c$ and the fault only affects the $\boldsymbol{L}_{\boldsymbol{b}}^{cc}$ block of $\boldsymbol{L}_{\boldsymbol{b}}$. This impacts both $\boldsymbol{P}_{\rm red}$ and $\boldsymbol{L}_{\rm red}$,

$$\begin{aligned} \boldsymbol{P}_{\rm red} &\to \boldsymbol{P}_{\rm red} - \delta(t)\,\tau\, b_{\alpha\beta}\frac{\boldsymbol{L}_{\boldsymbol{b}}^{gc}[\boldsymbol{L}_{\boldsymbol{b}}^{cc}]^{-1}\boldsymbol{e}_{(\alpha,\beta)}\boldsymbol{e}_{(\alpha,\beta)}^\top[\boldsymbol{L}_{\boldsymbol{b}}^{cc}]^{-1}\boldsymbol{P}_c}{1 - b_{\alpha\beta}\boldsymbol{e}_{(\alpha,\beta)}^\top[\boldsymbol{L}_{\boldsymbol{b}}^{cc}]^{-1}\boldsymbol{e}_{(\alpha,\beta)}}\,, \\ \boldsymbol{L}_{\rm red} &\to \boldsymbol{L}_{\rm red} - \delta(t)\,\tau\, b_{\alpha\beta}\frac{\boldsymbol{L}_{\boldsymbol{b}}^{gc}[\boldsymbol{L}_{\boldsymbol{b}}^{cc}]^{-1}\boldsymbol{e}_{(\alpha,\beta)}\boldsymbol{e}_{(\alpha,\beta)}^\top[\boldsymbol{L}_{\boldsymbol{b}}^{cc}]^{-1}\boldsymbol{L}_{\boldsymbol{b}}^{cg}}{1 - b_{\alpha\beta}\boldsymbol{e}_{(\alpha,\beta)}^\top[\boldsymbol{L}_{\boldsymbol{b}}^{cc}]^{-1}\boldsymbol{e}_{(\alpha,\beta)}}\,, \end{aligned} \tag{11}$$

where $\boldsymbol{e}_{(\alpha,\beta)} \in \mathbb{R}^{|\mathcal{N}_c|}$, and where we used the Sherman-Morrison formula (Sherman and Morrison, 1950)

$$\begin{aligned} [\boldsymbol{L}_{\boldsymbol{b}}^{cc} - b_{\alpha\beta}\boldsymbol{e}_{(\alpha,\beta)}\boldsymbol{e}_{(\alpha,\beta)}^\top]^{-1} &= [\boldsymbol{L}_{\boldsymbol{b}}^{cc}]^{-1} \\ &+ b_{\alpha\beta}\frac{[\boldsymbol{L}_{\boldsymbol{b}}^{cc}]^{-1}\boldsymbol{e}_{(\alpha,\beta)}\boldsymbol{e}_{(\alpha,\beta)}^\top[\boldsymbol{L}_{\boldsymbol{b}}^{cc}]^{-1}}{1 - b_{\alpha\beta}\boldsymbol{e}_{(\alpha,\beta)}^\top[\boldsymbol{L}_{\boldsymbol{b}}^{cc}]^{-1}\boldsymbol{e}_{(\alpha,\beta)}}\,, \end{aligned} \tag{12}$$

to express the inverse of the rank-1 correction of $\boldsymbol{L}_{\boldsymbol{b}}^{cc}$ in (4). The solution to the linearized swing equations with initial conditions $(\overline{\boldsymbol{\varphi}}_g(0), \overline{\boldsymbol{\omega}}_g(0)) = (0, 0)$ reads

$$\begin{bmatrix} \overline{\boldsymbol{\varphi}}_g(t) \\ \overline{\boldsymbol{\omega}}_g(t) \end{bmatrix} = e^{\boldsymbol{A}t} \underbrace{\begin{bmatrix} 0 \\ \frac{-b_{\alpha\beta}\,\tau\, \boldsymbol{M}^{-1/2}\boldsymbol{L}_{\boldsymbol{b}}^{gc}[\boldsymbol{L}_{\boldsymbol{b}}^{cc}]^{-1}\boldsymbol{e}_{(\alpha,\beta)}\boldsymbol{e}_{(\alpha,\beta)}^\top\boldsymbol{\theta}_c^\star}{1 - b_{\alpha\beta}\boldsymbol{e}_{(\alpha,\beta)}^\top[\boldsymbol{L}_{\boldsymbol{b}}^{cc}]^{-1}\boldsymbol{e}_{(\alpha,\beta)}} \end{bmatrix}}_{\boldsymbol{B}}, \tag{13}$$

where, again, we used rescaled angles and frequencies and $\boldsymbol{A}$ is given in (10).

The faulted line connects a synchronous machine and a passive node. In this case $\alpha \in \mathcal{N}_g$ and $\beta \in \mathcal{N}_c$, and the four blocks of $\boldsymbol{L}_{\boldsymbol{b}}$ change according to

$$\begin{aligned} \boldsymbol{L}_{\boldsymbol{b}}^{gg} &\to \boldsymbol{L}_{\boldsymbol{b}}^{gg} - b_{\alpha\beta}\,\hat{\boldsymbol{e}}_\alpha\hat{\boldsymbol{e}}_\alpha^\top\,, & \boldsymbol{L}_{\boldsymbol{b}}^{cc} &\to \boldsymbol{L}_{\boldsymbol{b}}^{cc} - b_{\alpha\beta}\,\hat{\boldsymbol{e}}_\beta\hat{\boldsymbol{e}}_\beta^\top\,, \\ \boldsymbol{L}_{\boldsymbol{b}}^{cg} &\to \boldsymbol{L}_{\boldsymbol{b}}^{cg} + b_{\alpha\beta}\,\hat{\boldsymbol{e}}_\beta\hat{\boldsymbol{e}}_\alpha^\top\,, & \boldsymbol{L}_{\boldsymbol{b}}^{gc} &\to \boldsymbol{L}_{\boldsymbol{b}}^{gc} + b_{\alpha\beta}\,\hat{\boldsymbol{e}}_\alpha\hat{\boldsymbol{e}}_\beta^\top\,, \end{aligned}$$

where $\hat{\boldsymbol{e}}_\alpha \in \mathbb{R}^{|\mathcal{N}_g|}$ and $\hat{\boldsymbol{e}}_\beta \in \mathbb{R}^{|\mathcal{N}_c|}$. $\boldsymbol{P}_{\rm red}$ and $\boldsymbol{L}_{\rm red}$ become respectively

$$\begin{aligned} &\boldsymbol{P}_{\rm red} - \delta(t)\,\tau\, b_{\alpha\beta}\frac{[\hat{\boldsymbol{e}}_\alpha + \boldsymbol{L}_{\boldsymbol{b}}^{gc}[\boldsymbol{L}_{\boldsymbol{b}}^{cc}]^{-1}\hat{\boldsymbol{e}}_\beta]\hat{\boldsymbol{e}}_\beta^\top[\boldsymbol{L}_{\boldsymbol{b}}^{cc}]^{-1}\boldsymbol{P}_c}{1 - b_{\alpha\beta}[L_b^{cc}]_{\beta\beta}^{-1}}\,, \\ &\boldsymbol{L}_{\rm red} - \delta(t)\,\tau\, b_{\alpha\beta}\frac{[\hat{\boldsymbol{e}}_\alpha + \boldsymbol{L}_{\boldsymbol{b}}^{gc}[\boldsymbol{L}_{\boldsymbol{b}}^{cc}]^{-1}\hat{\boldsymbol{e}}_\beta][\hat{\boldsymbol{e}}_\alpha^\top + \hat{\boldsymbol{e}}_\beta^\top[\boldsymbol{L}_{\boldsymbol{b}}^{cc}]^{-1}\boldsymbol{L}_{\boldsymbol{b}}^{cg}]}{1 - b_{\alpha\beta}[L_{\boldsymbol{b}}^{cc}]_{\beta\beta}^{-1}}\,. \end{aligned} \tag{14}$$

Again we used the Sherman-Morrison formula (12) to compute the inverse of $\boldsymbol{L}_{\boldsymbol{b}}^{cc} - b_{\alpha\beta}\hat{\boldsymbol{e}}_\beta\hat{\boldsymbol{e}}_\beta^\top$. Injecting (14) into (5), and solving the swing equations with initial conditions $(\overline{\boldsymbol{\varphi}}_g(0), \overline{\boldsymbol{\omega}}_g(0)) = (0,0)$ finally gives

$$\begin{bmatrix} \overline{\boldsymbol{\varphi}}_g(t) \\ \overline{\boldsymbol{\omega}}_g(t) \end{bmatrix} = e^{\boldsymbol{A}t} \underbrace{\begin{bmatrix} 0 \\ \frac{b_{\alpha\beta}\,\tau\,\boldsymbol{M}^{-1/2}(\hat{\boldsymbol{e}}_\alpha + \boldsymbol{L}_{\boldsymbol{b}}^{gc}[\boldsymbol{L}_{\boldsymbol{b}}^{cc}]^{-1}\hat{\boldsymbol{e}}_\beta)(\theta^\star_{g,\alpha} - \theta^\star_{c,\beta})}{1 - b_{\alpha\beta}[\boldsymbol{L}_{\boldsymbol{b}}^{cc}]^{-1}_{\beta\beta}} \end{bmatrix}}_{\boldsymbol{B}}, \tag{15}$$

where, again, we used rescaled angles and frequencies and $\boldsymbol{A}$ is given in Eq. (10).

With the above solutions to the swing equations, the performance measure $\mathcal{P}$ of (2) can be expressed as

$$\mathcal{P} = \boldsymbol{B}^\top \boldsymbol{X} \boldsymbol{B}\,, \tag{16}$$

with the observability Gramian $\boldsymbol{X} = \int_0^\infty e^{\boldsymbol{A}^\top t}\boldsymbol{Q}^{\mathrm{M}} e^{\boldsymbol{A}t}\mathrm{d}t$,

$$\boldsymbol{Q}^{\mathrm{M}} = \begin{bmatrix} \boldsymbol{M}^{-1/2}\boldsymbol{Q}^{(1,1)}\boldsymbol{M}^{-1/2} & 0 \\ 0 & \boldsymbol{M}^{-1/2}\boldsymbol{Q}^{(2,2)}\boldsymbol{M}^{-1/2} \end{bmatrix}, \tag{17}$$

and the matrices $\boldsymbol{A}$ and $\boldsymbol{B}$ obtained above in each of the three types of line fault, (9), (13) and (15).

For asymptotically stable systems (i.e. when all eigenvalues of $\boldsymbol{A}$ have negative real part), the observability Gramian $\boldsymbol{X}$ satisfies the Lyapunov equation

$$\boldsymbol{A}^\top \boldsymbol{X} + \boldsymbol{X}\boldsymbol{A} = -\boldsymbol{Q}^{\mathrm{M}}\,. \tag{18}$$

For Laplacian systems, $\boldsymbol{A}$ has a marginally stable mode, $\boldsymbol{A}[\boldsymbol{M}^{1/2}\boldsymbol{u}^{(1)}, 0]^\top = 0$. Here we follow the standard approach to deal with this marginally stable mode, which is to consider only performance measures $\boldsymbol{Q}$ such that $\boldsymbol{u}^{(1)} \in \ker(\boldsymbol{Q}^{(1,1)})$. In this case the observability Gramian is well defined by (18) with the additional constraint $\boldsymbol{X}[\boldsymbol{M}^{1/2}\boldsymbol{u}^{(1)}, 0]^\top = 0$ (Poolla et al., 2017). We are now ready to present our main result.

Proposition 1. **Primary control effort under line contingency.** Consider the Kron reduced power system model of (5), with $d_i/m_i \equiv \gamma$ and $m_i = m$, $\forall i \in \mathcal{N}_g$. The primary control effort $\mathcal{P} = \int_0^\infty \sum_i d_i\omega_i^2 \mathrm{d}t$ required during the transient caused by a line contingency modeled by (6) is given by

$$\mathcal{P} = \frac{P_{\alpha,\beta}^2\,\tau^2}{2}(m_\alpha^{-1} + m_\beta^{-1})\,, \tag{19}$$

if the faulted line connects two synchronous machines, by

$$\mathcal{P} = \frac{P_{\alpha,\beta}^2\,\tau^2}{2}\frac{\sum_{i\in\mathcal{N}_g} m_i^{-1}\left[\boldsymbol{e}_{(\alpha,\beta)}^\top \boldsymbol{L}_{\boldsymbol{b}}^{(cc)^{-1}}\boldsymbol{L}_{\boldsymbol{b}}^{(cg)}\hat{\boldsymbol{e}}_i\right]^2}{[1 - b_{\alpha\beta}\boldsymbol{e}_{(\alpha,\beta)}^\top[\boldsymbol{L}_{\boldsymbol{b}}^{(cc)}]^{-1}\boldsymbol{e}_{(\alpha,\beta)}]^2}\,, \tag{20}$$

if the faulted line connects two passive nodes, and by

$$\mathcal{P} = \frac{P_{\alpha,\beta}^2\,\tau^2}{2}\frac{\sum_{i\in\mathcal{N}_g} m_i^{-1}\left[\delta_{i\alpha} + \hat{\boldsymbol{e}}_\beta^\top \boldsymbol{L}_{\boldsymbol{b}}^{(cc)^{-1}}\boldsymbol{L}_{\boldsymbol{b}}^{(cg)}\hat{\boldsymbol{e}}_i\right]^2}{[1 - b_{\alpha\beta}[L_{\boldsymbol{b}}^{(cc)}]^{-1}_{\beta\beta}]^2}\,, \tag{21}$$

if the faulted line connects a synchronous machine α and a passive node β. In (19)–(21), $P_{\alpha,\beta} = b_{\alpha\beta}(\theta^\star_\alpha - \theta^\star_\beta)$ is the power flow on the $\alpha-\beta$ line prior to the fault.

Proof. The primary effort performance measure is given by (2) with $\boldsymbol{Q}^{(1,1)} = 0$ and $\boldsymbol{Q}^{(2,2)} = \boldsymbol{D}$. With (10), it is straighforward to see that the Lyapunov equation (18) has as solution an observability Gramian given by $\boldsymbol{X}^{(1,1)} = \boldsymbol{M}^{-1/2}\boldsymbol{L}_{\mathrm{red}}\boldsymbol{M}^{-1/2}/2$, $\boldsymbol{X}^{(2,2)} = \mathbb{I}/2$ and $\boldsymbol{X}^{(1,2)} = \boldsymbol{X}^{(2,1)} = 0$. To compute $\mathcal{P} = \boldsymbol{B}^\top\boldsymbol{X}\boldsymbol{B}$ for the above three types of lines contingencies, we note that only $\boldsymbol{X}^{(2,2)}$ matters and use $\boldsymbol{B}$ defined in Eqs. (9), (13) and (15) respectively. After some straightforward matrix multiplications, and rewriting the diagonal matrix of the synchronous machines inertia as $\boldsymbol{M}^{-1} = \sum_i m_i^{-1}\hat{\boldsymbol{e}}_i\hat{\boldsymbol{e}}_i^\top$ for $\hat{\boldsymbol{e}}_i \in \mathbb{R}^{|\mathcal{N}_g|}$, one obtains Eqs. (19), (20) and (21).

Eq. (19) shows that the effort of primary control which results from the outage of the $\alpha-\beta$ line is proportional to the square of the power flowing on the line prior to the fault times the prefactor $(m_\alpha^{-1} + m_\beta^{-1})$. The latter indicates that the primary control effort is large if the rotational inertias of the synchronous machines at both ends of the faulted line are small. For the other types of line contingencies, (20) and (21) predict a more involved dependence of $\mathcal{P}$ with the inertias of the synchronous machines, including topology-dependent factors. Quite interestingly, for both (20) and (21), only the inertias of the synchronous machines directly connected to the passive nodes matter. This is easily seen by noticing that for $\hat{\boldsymbol{e}}_i \in \mathbb{R}^{|\mathcal{N}_g|}$, $\boldsymbol{L}_{\boldsymbol{b}}^{(gc)}\hat{\boldsymbol{e}}_i = 0$ if the i^{th} synchronous machine is not connected to any of the passive nodes. The contribution of the inertias of the synchronous machines connected to the passive nodes is weighted by a network topology dependent term $\boldsymbol{L}_{\boldsymbol{b}}^{(cc)^{-1}}\boldsymbol{L}_{\boldsymbol{b}}^{(cg)}$. The denominator in (20) is smaller than one. It may actually be quite small, leading to large responses for initially moderately loaded lines for lines $\alpha-\beta$ between weakly connected components of the network of passive nodes. In particular, pairs of connected nodes (α,β) with only few, long alternative paths connecting them aside from the direct line $\alpha-\beta$ have values for $\boldsymbol{e}_{(\alpha,\beta)}^\top[\boldsymbol{L}_{\boldsymbol{b}}^{(cc)}]^{-1}\boldsymbol{e}_{(\alpha,\beta)}$ close to (but still smaller than) the resistance distance $\Omega_{\alpha\beta}$, which is close to the inverse line capacity $b_{\alpha\beta}^{-1}$. Remember however that "weakly connected" here still means "connected by at least two different paths", since the Sherman-Morrison formula applies to rank-1, nonsingular matrix corrections. In particular, it does not apply to single-line faults which split the network into two disconnected areas, the only case for which the denominator in (20) vanishes.

It is interesting to note that the primary control effort to restore synchrony, in the case of a nodal disturbance, only depends on the amplitude of the perturbation and on the inertia of the machine at the perturbed node, and not on the steady state operating conditions (Poolla et al., 2017). For line faults, our results show that the performance measure depends on the square of the power flowing on the line prior to the fault times an inertia dependent factor.

5. NUMERICAL ANALYSIS

We confirm our results numerically. We consider as physical network the IEEE 118-bus test case. We assume that all PQ buses are passive, and simulate the swing dynamics (5) on a network where all PQ buses have been eliminated by Kron reduction. To model temporary line disconnections, we consider time-dependent network Laplacians,

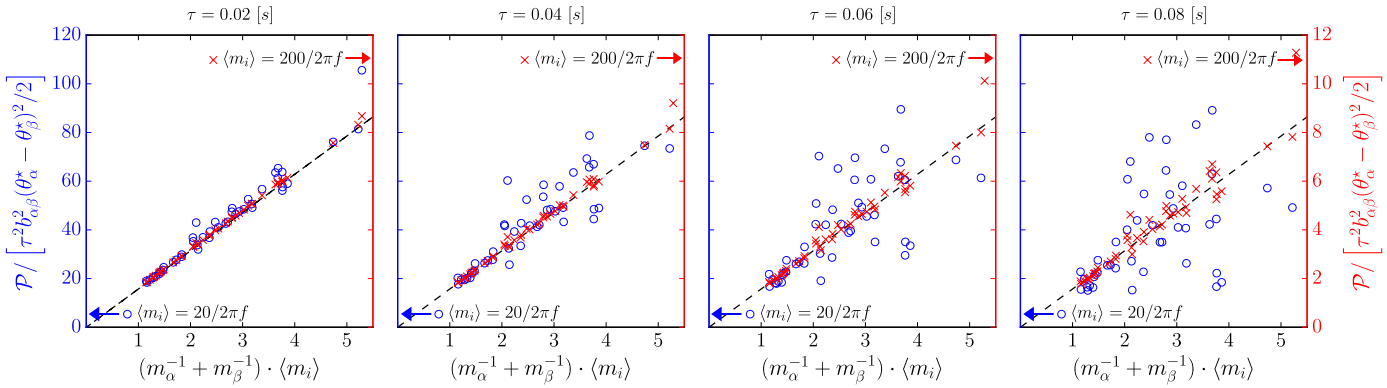

Fig. 1. Transient primary control effort for a line contingency as a function of the resistance distance separating the nodes of the faulted line. Each data point corresponds to the fault of a line connecting two generators in the physical network. Simulation parameters: IEEE 118-bus test case with inertias uniformly distributed in the interval $[0.2\langle m\rangle, 1.8\langle m\rangle]$ with $\langle m\rangle = 2H/2\pi f$, $H = 10$ $[s]$ (typical values from Kundur et al. (1994); blue circles, left vertical scale) and $\langle m\rangle = 200/2\pi f$ (exaggerated values to highlight the effect of inertia; red crosses, right vertical scale), $f = 50$ Hz, and $d_i/m_i = 0.5$ $[s^{-1}]$. From left to right: fault clearing times τ corresponding to $1, 2, 3$, and 4 AC cycles. The straight line gives our theoretical prediction Eq. (19).

$$\boldsymbol{L_b}(t) = \boldsymbol{L_b} - \Theta(t)\Theta(\tau - t) b_{\alpha\beta} \boldsymbol{e}_{(\alpha,\beta)} \boldsymbol{e}^\top_{(\alpha,\beta)}\,, \qquad (22)$$

where $\Theta(t)$ is the Heavyside step function, τ is the clearing time, and $\alpha - \beta$ is the faulted line. We perform numerical simulations for all possible line contingencies in the network. For each line contingency in the physical network we pre-compute the corresponding Kron reduced power injection $\boldsymbol{P}_{\rm red}$ and network Laplacian $\boldsymbol{L}_{\rm red}$ which we inject in the linearized swing equations (5) for the duration of the line fault. For each contingency simulation we evaluate numerically the primary effort performance measure $\int_0^\infty \sum_i d_i \omega_i^2(t) {\rm d}t$. We compare the numerical results to our theoretical predictions. Since the latter hold for Dirac-δ perturbations [see (6)], our theoretical results are expected to be accurate for small clearing times as $\delta(t) = \lim_{\tau\to 0} \Theta(t)\Theta(\tau - t)/\tau$.

Fig. 1, shows the behavior of the phase coherence measure rescaled by the square of the power flowing on the line prior to the fault for all lines connecting two synchronous machines in the physical network. For heterogeneous inertias and sufficiently short clearing times, (19) predicts

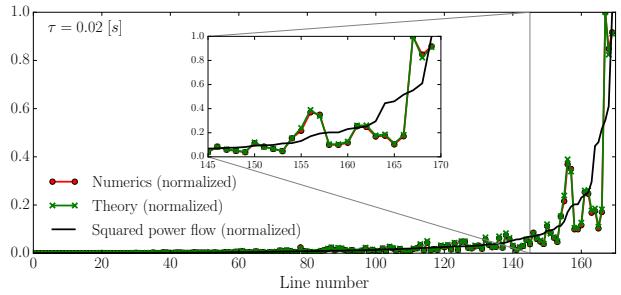

Fig. 2. Normalized primary control effort performance measure $\mathcal{P}/\mathcal{P}_{\rm max}$ (red), theoretical prediction (green), and square of the power flowing on the line prior to the fault (black) for line contingencies with clearing times $\tau = 0.02$ $[s]$, inertias uniformly distributed in the interval $[0.2\langle m\rangle, 1.8\langle m\rangle]$ with $\langle m\rangle = 2H/2\pi f$, $H = 10$ $[s]$, $f = 50$ Hz, and $d_i/m_i = 0.5$ $[s^{-1}]$. Transmission lines are ordered according to the power flowing on the line prior to the fault.

that this quantity scales linearly with $(m_\alpha^{-1} + m_\beta^{-1})$. This prediction is confirmed for sufficiently large inertias. For lower values of inertia, the linear tendency holds for short clearing times, but breaks down for longer faults. The validity of the observability Gramian prediction for Dirac-δ perturbations extends to longer clearing times for larger inertia of the synchronous machines (red crosses). This is so because for larger inertia, the voltage phase oscillations induced by the disturbance remain localized in the vicinity of the faulted line and do not have the time to propagate to distant nodes before the fault is cleared. These results show that for longer clearing times, and more generally for perturbations that are extended in time, alternative approaches to the observability Gramian are needed to accurately evaluate performance measures (Tyloo et al., 2018; Siami and Motee, 2016). Note that the red crosses in Fig. 1 correspond to somehow exaggerated values of inertia and are used here only to illustrate that our theoretical predictions remain valid for longer fault clearing times in the presence of larger inertias.

Fig. 2 shows the phase coherence measure for all possible line contingencies (170 lines in total, of which 46 connect two synchronous machines, 35 connect two passive nodes and 89 connect a passive node to a synchronous machine) and $\tau = 20$ ms. The transmission lines are sorted according to the square of the power flowing on the line in normal operation. Numerical results confirm that our theoretical predictions are accurate indicators of transient vulnerability under line contingency and that the transient excursion is given by the square of the power flowing on the transmission line prior to the fault, times a topological factor [See (20) and (21)].

Remarkably, our results show that the transient performance under line fault is not a monotonic function of the power load of the faulted line, the square of which is indicated by the black line in Fig. 2. Both the network topology and the distribution of inertia in the grid strongly impact the transients. We observe that the most critical lines are not always the most highly loaded ones. A fault on the line carrying the 3$^{\rm rd}$ largest power causes the largest

primary control effort, while a fault on the line carrying 44% of the largest transmitted power (the 14^{th} most loaded line) leads to the 4^{th} largest response. We saw (but do not show here) this non monotonic behavior also when lines are sorted according to their relative load (the load relative to their capacity).

6. CONCLUSION

The standard formalism used until now to evaluate performance measures of electric power grids was restricted to nodal perturbations (Tegling et al., 2015; Grunberg and Gayme, 2016; Poolla et al., 2017) and we extended it to line perturbations. We showed numerically that, despite its restriction to Dirac-δ perturbations (instantaneous in time), the formalism correctly evaluates performance measures even in the physically relevant case of perturbations with finite, but not too long duration. One would naively guess that the most critical lines are those that are the most heavily loaded, either relatively to their thermal limit or in absolute value. Quite surprisingly, we found that faults on lines transmitting less than half of the heaviest line load in the network sometimes require more primary control effort than lines with up to twice that load. This is so, because the performance measure (20)–(21) are given by the square of the original load on the faulted line times a term depending on the inertia and the topology of the network.

The performance measures we calculated could be used in $N-1$ contingeny analysis to quickly identify the most critical lines, based on topological characteristics of the network together with the load they carry. Future works should investigate nodal $N-1$ faults, where a bus with all its connected lines is removed from the network.

ACKNOWLEDGEMENTS

We thank B. Bamieh, F. Dörfler and M. Tyloo for useful discussions.

REFERENCES

Backhaus, S. and Chertkov, M. (2013). Getting a grip on the electrical grid. *Phys. Today*, 66(5), 42.

Bamieh, B., Jovanovic, M.R., Mitra, P., and Patterson, S. (2012). Coherence in large-scale networks: Dimension-dependent limitations of local feedback. *IEEE Transactions on Automatic Control*, 57(9), 2235.

Bamieh, B. and Gayme, D.F. (2013). The price of synchrony: Resistive losses due to phase synchronization in power networks. In *American Control Conference*, 5815. IEEE.

Coletta, T. and Jacquod, P. (2017). Resistance distance criterion for optimal slack bus selection. *arXiv:1707.02845*.

Dörfler, F. and Bullo, F. (2013). Kron reduction of graphs with applications to electrical networks. *IEEE Transactions on Circuits and Systems I*, 60(1), 150.

Fardad, M., Lin, F., and Jovanovic, M.R. (2014). Design of optimal sparse interconnection graphs for synchronization of oscillator networks. *IEEE Transactions on Automatic Control*, 59(9), 2457.

Grunberg, T.W. and Gayme, D.F. (2016). Performance measures for linear oscillator networks over arbitrary graphs. *IEEE Transactions on Control of Network Systems*, PP(99), 1.

Klein, D.J. (1997). Graph geometry, graph metrics and Wiener. *Commun. Math. Comput. Chem.*, 35, 7.

Klein, D.J. and Randić, M. (1993). Resistance distance. *Journal of Mathematical Chemistry*, 12(1), 81.

Kou, G., Hadley, S., Markham, P., and Liu, Y. (2013). Developing generic dynamic models for the 2030 eastern interconnection grid. URL `http://www.osti.gov/scitech/`.

Kundur, P., Balu, N.J., and Lauby, M.G. (1994). *Power system stability and control*, volume 7. McGraw-hill New York.

Kuramoto, Y. (1975). Self-entrainment of a population of coupled non-linear oscillators. *Lecture Notes in Physics*, 39, 420.

Machowski, J., Bialek, J.W., and Bumby, J.R. (2008). *Power system dynamics: stability and control*. John Wiley.

Paganini, F. and Mallada, E. (2017). Global performance metrics for synchronization of heterogeneously rated power systems: The role of machine models and inertia. *arXiv:1710.07195*.

Pikovsky, A., Rosenblum, M., and J, K. (2001). *Synchronization: A Universal Concept in Nonlinear Sciences*. Cambridge University Press.

Poolla, B.K., Bolognani, S., and Dörfler, F. (2017). Optimal placement of virtual inertia in power grids. *IEEE Transactions on Automatic Control*, PP(99), 1.

Rohden, M., Sorge, A., Witthaut, D., and Timme, M. (2014). Impact of network topology on synchrony of oscillatory power grids. *Chaos*, 24, 013123.

Sherman, J. and Morrison, W.J. (1950). Adjustment of an inverse matrix corresponding to a change in one element of a given matrix. *Ann. Math. Statist.*, 21(1), 124.

Siami, M. and Motee, N. (2016). Fundamental limits and tradeoffs on disturbance propagation in linear dynamical networks. *IEEE Transactions on Automatic Control*, 61(12), 4055.

Stephenson, K. and Zelen, M. (1989). Rethinking centrality: Methods and examples. *Social Networks*, 11(1), 1.

Summers, T., Shames, I., Lygeros, J., and Dörfler, F. (2015). Topology design for optimal network coherence. In *European Control Conference*, 575. IEEE.

Tegling, E., Bamieh, B., and Gayme, D.F. (2015). The price of synchrony: Evaluating the resistive losses in synchronizing power networks. *IEEE Transactions on Control of Network Systems*, 2(3), 254.

Tyloo, M., Coletta, T., and Jacquod, P. (2018). Robustness of synchrony in complex networks and generalized kirchhoff indices. *Phys. Rev. Lett.*, 120, 084101.

Xiao, W. and Gutman, I. (2003). Resistance distance and laplacian spectrum. *Theoretical Chemistry Accounts*, 110(4), 284.

Zhou, K., Doyle, J., and Glover, K. (1996). Robust and optimal control.